Impact of skin effect on single-well push-pull tests with the presence of regional groundwater flow

Xu Li[a], Zhang Wen[a]*, Hongbin Zhan[a,b], Qi Zhu[a]

Manuscript submitted to *Hydrology and Earth System Sciences*

[a]School of Environmental Studies, China University of Geosciences, Wuhan, 430074, China

[b]Department of Geology and Geophysics, Texas A & M University, College Station, TX 77843-3115, USA, Email: zhan@geo.tamu.edu

*Corresponding author: Zhang Wen, Ph.D. Professor. Affiliation: School of Environmental Studies, China University of Geosciences, Wuhan, Hubei, 430074, P. R. China. Email: wenz@cug.edu.cn. Tel: 86-27-67883159. Fax: 86-27-87436235.

Abstract

Single-well push-pull (SWPP) test is one of the most important ways to estimate aquifer transport parameters, e.g. porosity, dispersivity, ~~the~~ regional groundwater velocity~~rate of biogeochemical reaction, but its application for determining the regional groundwater velocity has rarely been discussed in previous studies~~. ~~A~~The wellbore is surrounded by a finite-thickness skin, such as a gravel pack usually, thus the aquifer can be regarded as a radial two-zone system. If the hydraulic conductivity of the skin is smaller than that of the aquifer formation zone, the skin is defined as a positive one. Otherwise, it is a negative skin. In this study, a ~~new~~ numerical model of SWPP test considering ~~regional groundwater flow and~~ skin effects was established using the finite-element COMSOL Multiphysics software to estimate aquifer transport parameters. ~~The effects of regional groundwater flow velocity and skin properties on breakthrough curves (BTCs) were thoroughly analyzed.~~ Several important results were obtained. Firstly, ~~the~~ different regional groundwater velocity affects the types of breakthrough curves (BTCs~~) through changing the pattern and location of the dividing streamline~~. Secondly, a positive (or negative) skin leads to a slower (or faster) tracer transport process, and~~. That is, a positive skin results in a higher concentration at early stage at a given time.~~ ~~Thirdly,~~ a smaller ratio between the hydraulic conductivity of the skin and that of the aquifer formation~~a smaller hydraulic conductivity ratio δ of the positive skin to the formation~~ results in greater solute plume retardation in the skin zone. Thirdly, ~~Besides,~~ a larger thickness of the positive skin leads to a higher tracer concentration around the well. The opposite is true if the skin is negative. Besides, ~~the~~ different hydraulic conductivities and skin thickness can result in different ratios of tracer mass recovered during the pumping phase.

The general conclusion is that the skin effects on SWPP test are significant and should be considered.

Keywords: push-pull test, regional groundwater velocity, solute transport, skin effect

1. Introduction

The single-well push-pull (SWPP) tests have been commonly employed to estimate aquifer parameters, e.g. ~~regional groundwater flow velocity,~~ porosity, dispersivity, biogeochemical reaction rate (Gelhar and Collins, 1971; Hall et al., 1991; Schroth and Istok, 2006; Johnsen~~,~~ et al., 2009). The process of this test can be summarized as follows: A tracer is injected into a target aquifer (injection phase~~push~~), then the mixed solution is pumped out from the same location (~~pull~~pumping phase). Groundwater samples are taken at regular time intervals at the test well during the pumping process, and parameters can be obtained by fitting the observed breakthrough curves (BTCs) using a proper mathematical model. ~~Generally, a complete SWPP test may consist of four phases: tracer injection, chasing, rest, and pumping. The chasing phase is to push the tracer away from the injection well (Istok et al., 1997), and the rest phase is for tracer to diffuse and/or react with the aquifer (if a reactive tracer is employed).~~ Conservative or reactive tracers can be utilized, depending on the purpose of the test. In general, conservative tracers have been widely used to estimate regional groundwater flow velocity, porosity, and dispersivity, etc. (Leap and Kaplan, 1988; Haggerty et al., 2001; Hebig-Schubert, 2014). Similarly, one can obtain the information of sorption, cation exchange, microbial processes by applying reactive tracers (Trudell et al., 1986; Field et al., 2000; Tong et al., 2016). For instance, Tong et al. (2016) used SWPP tests to validate the abundant production of hydroxyl radicals due to the oxidization of subsurface sediments.

To interpret the SWPP test results, a proper mathematical model considering the fundamental physical and biogeochemical processes of the test is indispensable (Haggerty et

al., 2001; Kleikemper et al., 2002; Schroth and Istok, 2006). From a transport perspective, many existing models are governed by the conventional advection-dispersion equation (ADE), assuming the validity of Fick's law in the SWPP tests (Schroth et al., 2000; Huang et al., 2010). Subsequently, many analytical and numerical solutions of various single-well models have been developed. For instance, Huang et al. (2010) obtained an exact analytical solution of SWPP test by using Fick's law, considering a partially penetrating well in the aquifer. Besides ADE, a number of non-Fickian transport models of SWPP tests have also been developed in recent years to recognize the influence of media heterogeneity, especially in fractured aquifers (Chen et al., 2017). Such models include multi-rate mass transfer models (Haggerty et al., 2001, Hansen et al., 2016), continuous time random walk (CTRW) (Le Borgne and Gouze, 2008), and fractional advection-dispersion equation (FADE) models (Benson et al., 2004; Chen et al., 2017), to name a few. For instance, Chen et al. (2017) developed a fractional model of multistage SWPP test to simulate non-Fickian behavior for a fractured aquifer. In addition, Schroth et al. (2005) obtained an approximate analytical solution of SWPP test for spherical-flow conditions. Wang et al. (2017) investigated the impacts of transient flow and wellbore storage on SWPP test under transient Forchheimer flow using a finite-difference method.

As mentioned above, SWPP test is a powerful tool for aquifer characterization, but its application for determining the regional groundwater velocity has rarely been discussed in previous studies~~including the determination of regional groundwater flow velocity~~. The groundwater flow velocity may be measured directly using a two-well tracer test conducted under nature gradient condition, but this requires a monitoring well that is located directly

down-gradient at a convenient distance from the test well, which is unlikely in most field applications (as one may not be aware of the hydraulic gradient and groundwater flow direction before the installation of monitoring wells). In fact, in most cases, the hydraulic gradient is determined using a three-well triangle and the groundwater flow velocity (including its magnitude and direction) may be obtained if the hydraulic conductivity and effective porosity are also known. If the hydraulic conductivity and effective porosity are unavailable, one may rely on the BTCs obtained from such a three-well system in a natural gradient tracer test as an alternative to determine the regional flow velocity and longitudinal and transverse dispersivities as well. This is can be done using the following procedures. First, the direction of hydraulic gradient can be determined based on the hydraulic head measurements in three monitoring wells, and the groundwater flow direction is directly opposite of the hydraulic gradient direction in a horizontally isotropic media (which is usually true for most field applications). Second, after determining the direction of groundwater flow, one has three more parameters to determine: the magnitude of the groundwater flow velocity and longitudinal and transverse dispersivities. Such three unknown parameters can be obtained using the concentrations measured in above three (or more) wells~~As we know, it is difficult to guarantee a directly down-stream gradient monitoring well at a convenient distance from the test well in field condition ,~~ ~~Traditionally~~therefore~~, regional groundwater flow velocity can be obtained by three or more groundwater monitoring wells in the aquifer~~ by conducting the natural gradient tracer tests rather than the SWPP tests (Pickens et al., 1981; Michie, 1996; Zimmermann and Huenges~~-~~, 1999).

However, the natural gradient tracer tests usually take much longer time to complete. This is particularly troublesome when the medium is less permeable, and the regional groundwater flow velocity is relatively small (Schubert et al., 2011). The natural gradient tracer test method is also very costly to implement in deep aquifers as the installation of multiple wells in deep aquifers can be formidably expensive. In contrast, the SWPP test only needs a single well, thus can substantially reduce the cost of test, and becomes a nice alternative for the determination of regional groundwater flow velocity (Leap and Kaplan, 1988; Butler et al., 2009). To serve such a purpose, the SWPP test~~s~~ usually consist of three phases: tracer injection, drift ~~rest~~, and pumping, is different from the traditional SWPP test model. The drift~~rest~~ phase allows the injected tracer to drift with regional groundwater velocity, thus it is a key phase to include. Leap and Kaplan (1988) obtained an equation for push-pull test to determine regional groundwater flow velocity in a confined aquifer, and a series of laboratory tests were conducted to verify the accuracy of the model, ~~but~~ and they described a "velocity shadow" that exists for some distance down~~ stream~~ gradient of the well. Hall et al. (1991) considered that~~the test results showed that~~ if the ~~solute transport~~tracer was not drifted over~~ the location of dividing streamline to~~ the~~ward downstream,~~ "velocity shadow" before pumping, the calculated results of the regional flow velocity would produce a ~~large~~ small error with the comparison to the actual value. After that, Monkmeyer and Netzer (1993) in their comment on the paper of Leap and Kaplan (1998), firstly considered a stagnation point (where groundwater velocity is zero) during a SWPP pumping phase, and they considered that the tracer can be recovered, if the tracer was not drifted over stagnation point at the edge of the capture zone. Recently, Charles et al. (2018) conducted a SWPP test in unconfined

aquifer, and estimated effective porosity and regional groundwater flow velocity, by using modified equations of Leap and Kaplan (1988). ~~Hall et al. (1991) presented another type of SWPP test for determining regional groundwater velocity and effective porosity based on the method of Leap and Kaplan (1988), but Hall et al. (1991) required a directly downgradient monitoring well. It is notable that both approaches mentioned above have some limitations for determining regional groundwater velocity.~~

In addition, the impacts of skin near a pumping well are usually neglected for a SWPP test, which might bring about great errors for the estimation of aquifer parameters and regional groundwater flow velocity. During the process of well implementation, the intrusion of drilling mud into the aquifer in the vicinity of well is inevitable, which can result in the change of the porosity and permeability surrounding the well screen (Hurst et al., 1969). This phenomenon can be regarded as the skin effect (Chen and Chang, 2002; Wang et al., 2012). The thickness of skin usually ranges from a few millimeters to several meters (Novakowski, 1989). The skins can be classified into positive and negative types according to the hydraulic conductivity contrast between the skin and the aquifer formation zone. If the hydraulic conductivity of the skin is smaller than that of the aquifer formation zone, the skin is defined as a positive one. Otherwise, it is a negative skin (Park and Zhan, 2002; Yeh et al., 2003; Wen et al., 2011). Such a skin, regardless of positive or negative, will inevitably alter the flow field near the test well, thus its effect must be taken into consideration for interpreting the SWPP test. For instance, the streamlines of skin zone can converge toward the well in the case of a negative skin, but the opposite is true for a positive skin (Drost et al., 1968; Schubert et al., 2011).

In summary, the skin effect is a very important issue from the perspective of SWPP test interpretation. Through a careful check on the literature, we notice that the model of SWPP for estimating groundwater flow velocity needs further investigation, besides, the impacts of skin effects on SWPP tests for estimating groundwater flow velocity have rarely been studied, which will be the purpose of this study. To accomplish the objective, we will investigate a SWPP test containing three phases of injection, rest and pumping using a fully penetrating well. We will use the finite-element COMSOL Multiphysics to numerically simulate the steady-state, two-dimensional (2D) horizontal flow, with specific attention paid to the skin effect.

2. Mathematical model of the SWPP test

To illustrate the problem, we will use a conservative tracer. A confined aquifer is assumed to be unbounded laterally with a uniform regional groundwater flow presented over the entire duration of test. The aquifer is assumed to be homogeneous and horizontally isotropic. A fully penetrating well is used so only the horizontal flow is of concern here. Flow is assumed to be Darcian and transport is assumed to be Fickian. The test well radius (r_w) is assumed to be sufficiently small so that the wellbore ~~effect~~ storage is not a concern. The tracer is injected with a constant rate and a constant concentration at the injection phase and is pumped with a constant rate (which could be different from the injection rate) at the pumping phase, after a certain period of ~~rest~~ drift phase to allow the injected tracer drifting with the regional groundwater flow. The coordinate system is established as follows with the origin at the center of the test well and the *x*-axis pointing to the direction of regional groundwater flow. A 2D schematic diagram investigated here is depicted in Fig.1. The

confined aquifer consists of two zones in the radial direction. The first zone, known as the wellbore skin zone, is located around the injection well and has a thickness of r_{sw}-r_{ws}, where r_s is skin radius. The second zone is known as the aquifer formation zone.

2.1 Mathematical model of groundwater flow

Flow of the SWPP test is assumed to be steady-state, thus the groundwater flow velocity of the skin zone can be expressed as the superposition of the flow component generated by the pumping well and the regional flow:

$$\vec{v}_1 = \vec{v}_{r1} + \vec{v}_{x1} \quad (1)$$

$$\vec{v}_{r1} = v_{r1}\vec{e}_r = Q/(2\pi\theta_s Br)\vec{e}_r \quad (2)$$

$$\vec{v}_{x1} = v_{x1}\vec{e}_x = (-K_s J_s/\theta_s)\vec{e}_x = (v_{d1}/\theta)\vec{e}_x \quad (3)$$

$$r = \sqrt{x^2 + y^2} \quad (4)$$

where the arrow over a symbol represents a vector hereinafter; $\vec{v}_{r1}$ is the average radial pore velocity vector of the skin zone generated by the injection (or pumping well) with a magnitude of v_{r1} [L/T]and $\vec{e}_r$ is a unit vector along the radial direction; $\vec{v}_{x1}$ is the regional groundwater pore flow velocity vector of the skin zone with a magnitude of ~~v_2~~-v_{x1} [L/T] and v_{d1} is the regional groundwater Darcy flow velocity of the skin zone, and $\vec{e}_x$ is a unit vector long the x-axis; $\vec{v}_1$ is the lumped groundwater flow velocity ~~near the well~~in the skin zone [L/T]; B is the aquifer thickness [L]; ~~r is the radial distance [L];~~ Q is the injection or pumping rate [L^3/T], which is positive for the injection and negative for pumping, and Q is 0 during the ~~rest~~ drift phase; K_s is ~~aquifer~~ hydraulic conductivity of the skin zone [L/T]; J_s is the hydraulic gradient of regional flow in the skin zone[L/L]; θ_s is the ~~aquifer~~ effective porosity of the skin zone [dimensionless], which is assumed to be the same as the total porosity of the

域代码已更改

域代码已更改

aquifer when all the pore spaces are well-connected with negligible immobile porosity; r is the radial distance [L] from the well and x and y are two horizontal coordinates [L], parallel and perpendicular to the regional groundwater flow direction, respectively.

In addition, the groundwater flow velocity ~~of~~in the aquifer formation zone can be expressed as:

$$\vec{v}_2 = \vec{v}_{r2} + \vec{v}_{x2} \quad (5)$$

$$\vec{v}_{r2} = v_{r2}\vec{e}_r = Q/(2\pi\theta Br)\vec{e}_r \quad (6)$$

$$\vec{v}_{x2} = v_{x2}\vec{e}_x = (-KJ/\theta)\vec{e}_x = (v_{d2}/\theta)\vec{e}_x \quad (7)$$

where $\vec{v}_{r2}$ is the average radial pore velocity vector of the aquifer formation zone generated by the injection (or pumping well) with a magnitude of v_{r2} [L/T]; $\vec{v}_{x2}$ is the regional groundwater pore flow velocity vector of the aquifer formation zone with a magnitude of v_{x2} [L/T] and v_{d2} is the regional groundwater Darcy flow velocity of the aquifer formation zone; $\vec{v}_2$ is the lumped groundwater flow velocity in the aquifer formation zone [L/T]; K is the aquifer hydraulic conductivity [L/T]; J is the hydraulic gradient of regional flow in the aquifer formation zone [L/L]; θ is the aquifer effective porosity [dimensionless].

~~According to Fig.1, the boundary conditions for the domain of concern can be expressed as:~~

~~$$H(x,y)\big|_{s_1} = H_1, \quad H(x,y)\big|_{s_2} = H_2 \quad (5)$$~~

~~$$K\frac{\partial H}{\partial n}\Big|_{s_3} = 0, \quad K\frac{\partial H}{\partial n}\Big|_{s_4} = 0 \quad (6)$$~~

~~where s_1, s_2, s_3 and s_4 are the boundaries of the model; s_1 and s_2 are constant-head boundaries with prescribed heads of H_1 and H_2, respectively; both s_3 and s_4 are no-flux boundaries.~~

域代码已更改
域代码已更改
域代码已更改
域代码已更改
域代码已更改
域代码已更改

~~Therefore, a constant regional flow field can be generated and one can obtain different values of v_2 by changing the head differences of H_1 and H_2.~~

2.2 Mathematical model of solute transport

The solute transport is dominated by advection and dispersion in the two-zone system.

The ADE of a conservative solute in the skin zone without source/sink can be written as:

$$\frac{\partial C_1}{\partial t} = \nabla \cdot \left(D \nabla C_1\right) - \nabla \cdot \left(\vec{v}_1 C_1\right), \quad r_w < r \le r_s, t > 0 \qquad (7\text{-}8)$$

and in the aquifer formation zone as:

$$\frac{\partial C_2}{\partial t} = \nabla \cdot \left(D \nabla C_2\right) - \nabla \cdot \left(\vec{v}_2 C_2\right), \quad r_s < r < \infty \qquad (9)$$

域代码已更改

where C_1 and C_2 are solute concentrations in the skin and aquifer formation zones, respectively [M/L^3]~~C is the solute concentration [M/L^3]~~; t is the transport time [T]; D_1 is the hydrodynamic dispersion [L^2/T]; $\nabla\cdot$and ∇ are the divergence operator and the gradient operator respectively; the hydrodynamic dispersion is a velocity-dependent tensor depicted as:

$$D_{xx} = \frac{\alpha_L v_x^2}{\left|\vec{v}\right|} + \frac{\alpha_T v_y^2}{\left|\vec{v}\right|} + D_{diff} \qquad (8\text{-}10)$$

$$D_{yy} = \frac{\alpha_L v_y^2}{\left|\vec{v}\right|} + \frac{\alpha_T v_x^2}{\left|\vec{v}\right|} + D_{diff} \qquad (9\text{-}11)$$

$$D_{xy} = D_{yx} = \left(\alpha_L - \alpha_T\right)\frac{v_x v_y}{\left|\vec{v}\right|} \qquad (10\text{-}12)$$

$$v = \sqrt{v_x^2 + v_y^2} \qquad (11\text{-}13)$$

where D_{xx}, D_{xy}, and D_{yy} are components of the hydrodynamic dispersion coefficient tensor [L^2/T]; D_{diff} is the molecular diffusion coefficient [L^2/T]; α_L is the longitudinal dispersivity [L]; α_T~~–~~ is the transverse dispersivity [L]; the transverse dispersion effect is much smaller,

thus one usually assumes $\alpha_L = 10\alpha_T$ (Guvanasen and Guvanasen, 1987; Chen et al., 1999; Chen et al., 2006); v_x is pore velocity in the x direction; v_y is pore velocity in the y direction.

The initial condition is:

$$C_1(r,0) = C_2(r,0) = 0, \quad r \geq r_w, \tag{12}$$

During the injection phase, the inner boundary condition inside the well can be described as:

$$C_1(r,t) = C_0, \quad r = r_w, 0 < t < t_{inj} \tag{13}$$

where C_0 represents the concentration of the injection phase [M/L^3]; r_w is the well radius [L]; t_{inj} is the duration of the injection phase [T]. The third-type boundary condition may also be used to replace the first-type boundary condition of Eq. (13). However, our numerical exercises indicate that both conditions yield nearly the same results except for a very short period of time since the start of injection. Therefore, without loss of generality, we use the first-type boundary condition here as an example to illustrate the methodology.

During the rest phase, the solute flux from the borehole into the aquifer is zero, but the solute concentration around the borehole is nonzero, therefore, rather than a constant concentration boundary, a constant-flux (or the third-type) boundary is more reasonable and can be described as:

$$v_1 C - D \left. \frac{\partial C}{\partial r} \right|_{r \to r_w^-} = 0, \quad t_{inj} < t < t_{res}. \tag{14}$$

where t_{res} is the duration of the rest phase [T]. Eq. (14) represents a zero-flux boundary. During the rest phase, Q is 0.

During the pumping phase, the time-dependent concentration is measured in the borehole. The main target of the test is to obtain several parameters by fitting the observed

~~breakthrough curves (BTCs) with corresponding theoretical BTCs obtained from a proper analytical or numerical solution. When solute transport through well screen, the boundary condition at the well screen is (Wang et al., 2017):~~

~~$$\left.\frac{\partial C}{\partial r}\right|_{r\to r_w^-}=0 \quad (15)$$~~

~~Because the values of velocity and concentration are different around the perimeter of the borehole, it is necessary to integrate the concentration around the borehole with the velocity as the weight to obtain the accurate value of concentration at the well, thus, the flux averaged concentrations can be expressed as:~~

~~$$\overline{C}=\frac{\oint_{l_w} v_w C_w}{\oint_{l_w} v_w},\quad r=r_w, t_{res}<t<t_{pump} \quad (16)$$~~

~~where v_w represents the superposition velocity around the borehole during the pumping [L/T]; C_w represents the concentration around the well perimeter [M/L3]; $\overline{C}$ is the concentration inside the well [M/L3]; l_w is the perimeter of the wellbore [L].~~

3. Numerical solution of the SWPP test

In this study, a steady-state flow model of 2D horizontal plane was developed based on COMSOL Multiphysics, as shown in Fig. 1. The model region was set to be 40 m×40 m, and the well has a radius of 0.1 m. In addition, B=10 m, K=8.0 m/d, θ=0.3. According to Fig.1, the boundary conditions for the domain of concern can be expressed as:

$$H(x,y)\big|_{s_1}=H_1,\ H(x,y)\big|_{s_2}=H_2 \quad (14)$$

$$K\frac{\partial H}{\partial n}\Big|_{s_3}=0,\ K\frac{\partial H}{\partial n}\Big|_{s_4}=0 \quad (15)$$

域代码已更改
域代码已更改
域代码已更改
域代码已更改

where s_1, s_2 ,s_3 and s_4 are the boundaries of the model; s_1 and s_2 are constant-head boundaries with prescribed total heads of $H_1$and H_2, respectively; both s_3 and s_4 are no-flux boundaries; n is the normal vector of the boundary (an outward pointing vector perpendicular to the boundary). Therefore, a constant regional flow field can be generated and one can obtain different values of v_{x2} by changing the head differences of H_1 and H_2. In this model, constant-head boundaries were prescribed, and the value of H_2 was set as constant 15 m, according to Eq. (~~3~~7), one can obtain different values of v_{x2} by changing the value of H_1. In the model, a continuous mass flux of injection or pumping rate was assigned at $r=r_w$, which can be expressed as:

$$N_0 = \frac{Q\rho}{2\pi r_w B} \quad (~~17~~16)$$

where, N_0 is the mass flux per unit thickness [M/L^2/T]; ρ is the density of groundwater [M/L^3]. ~~The SWPP test was divided into three phases, the simulation results at the end of each phase, including the hydraulic head and the solute concentration, were set as the initial values for the simulation in the next phase.~~

A uniform skin near the well was considered in a confined aquifer, and the~~–~~ well skin thickness of r_{sw}-r_{ws} the well skin was assumed to be constant~~– and equal to r_s along the well screen~~ in this model. The skin hydraulic conductivity and effective porosity were set as K_s and θ_s respectively. The default values of the parameters were shown in Table 1.

For the solute model, the initial condition in both the skin and aquifer formation zones are:

$$C_1(r,0) = C_2(r,0) = 0, \ r \geq r_w, \quad (17)$$

域代码已更改

During the injection phase, the boundary condition at $r=r_w$ can be described as:

$$C_1(r,t) = C_0, \qquad r = r_w, 0 < t < t_{inj} \tag{18}$$

where C_0 represents the concentration of the injection phase [M/L^3]; t_{inj} is the duration of the injection phase [T]. The third-type boundary condition may also be used to replace the first-type boundary condition of Eq. (20). However, our numerical exercises indicate that both conditions yield nearly the same results except for a very short period of time since the start of injection. Therefore, without loss of generality, we use the first-type boundary condition here as an example to illustrate the methodology.

The concentration and the flux at the interface between the skin and aquifer formation zones are continuous, can be expressed as:

$$C_1(r_s,t) = C_2(r_s,t), \ t > 0 \tag{19}$$

and

$$D\frac{\partial C_1(r_s,t)}{\partial} = D\frac{\partial C_2(r_s,t)}{\partial}, \ t > 0 \tag{20}$$

During the pumping phase, the time-dependent concentration is measured in the borehole. The main target of the test is to obtain several parameters by fitting the observed ~~breakthrough curves (~~BTCs~~)~~ with corresponding theoretical BTCs obtained from a proper analytical or numerical solution. When solute transport through well screen, the boundary condition at the well screen is (Wang et al., 2017):

$$\left.\frac{\partial C}{\partial r}\right|_{r \to r_w^-} = 0 \tag{21}$$

Because the values of velocity and concentration are different around the perimeter of the borehole, it is necessary to integrate the concentration around the borehole with the

域代码已更改

域代码已更改

域代码已更改

域代码已更改

velocity as the weight to obtain the accurate value of concentration at the well, thus, the flux-averaged concentrations can be expressed as:

$$\overline{C}_{pump} = \frac{\oint_{l_w} v_w C_w}{\oint_{l_w} v_w}, \qquad r = r_w, t_{res} < t < t_{pump} \tag{22}$$

where v_w represents the ~~superposition~~ velocity around the borehole during the pumping [L/T]; C_w represents the concentration around the well perimeter [M/L3]; $\overline{C}$ is the concentration inside the well [M/L3]; l_w is the perimeter of the wellbore [L]. The SWPP test was divided into three phases, the simulation results at the end of each phase, including the hydraulic head and the solute concentration, were set as the initial values for the simulation in the next phase.

域代码已更改

域代码已更改

The model domain was discretized into 21688 elements, and the mesh size was progressively refined near the well, and the well perimeter was discretized into 28 elements. When the number of element is doubled, the peak solute concentration for the pumping phase varied about 0.17%. Therefore the selected mesh is regarded as sufficiently fine for the problem investigated here. To check the accuracy of the numerical model further, the numerical solution for a special case (without skin) was used to compare with the analytical solution of Huang et al. (2010), who investigated a steady-state flow SWPP model with injection and extraction phases, without the regional groundwater flow, as shown in Fig.2. The simulated time span of tracer injection and pumping were 0.5 and 1 day, respectively. The other parameters were given as: Q_{inj}= 50 m^3/d, Q_{pump}=-50 m^3/d, B=10 m, α_L=0.1 m, 0.5 m, 1 m, and θ=0.3. C_0 at r=r_w was set as 1.0 mol/m^3. The results showed that our numerical solution agreed perfectly with the analytical solution. For the following analysis, the default values of the parameters are listed in Table 1.

4. Results and discussions

4.1. ~~Effects of regional groundwater velocity on BTCs in the SWPP test~~Types of breakthrough curves for different regional groundwater velocity

The main target of this SWPP test is to estimate the unknown regional groundwater velocity. In order ~~T~~to interpret the BTCs, a parametric study over a wide range of regional groundwater velocities ~~is~~was conducted. Fig. 3 shows the BTCs for the pumping phase with different regional groundwater velocities, like 5×10^{-7} m/s, 1×10^{-6} m/s, 1.5×10^{-6}m/s, 2×10^{-6} m/s, 2.5×10^{-6} and 3×10^{-6} m/s. Besides, α_L =0.1 m, Q_{inj}= 30 m^3/d, Q_{pump}=-15 m^3/d, and the other parameters are the same as those used in Table 1. It is found that different regional groundwater velocities have great impacts on BTCs, and such impacts depend on the value of the regional groundwater velocities. It is found that the tracer concentration is smaller at early stage with a greater regional groundwater velocity. Additionally, it is notable that a larger regional groundwater velocity will result in a longer tailing.

Fig. 4 shows the superposition of flow components generated by the pumping well and the regional flow. A minor point to note is that Figure 4 only shows a flow pattern for a small area nearby the well, not for the entire domain, thus the streamlines there appear not orthogonal to the upper and lower boundaries. For the pumping phase, one can see that there is a stagnation point (Sp), where the groundwater velocity (v_2) is zero, located at the dividing streamline (Ds) or envelope of the capture zone as shown in Fig.4. The Ds divides the flow into the capture zone and the non-capture zone, while ~~and~~ the Sp represents the uppermost location downgradient from the pumping well inside a capture zone ~~the edge of the capture zone along a directly downgradient direction~~. ~~For a single tracer particle,~~ If the tracer does

not drift beyond ~~(with the regional flow only) over~~ the ~~edge~~stagnation point of the capture zone during the drift phase, ~~whether~~ it can be extracted ~~out~~ from the aquifer ~~depends on the pattern and location of the dividing line~~, which acts like a fishing net to collect all the products together. Therefore, different convergence situations of tracer due to variable dividing streamlines result in a series of BTC types. In order to interpret this behavior explicitly, the concentration distributions in a 2D horizontal plane at t_{pump}=0 hr with different regional groundwater velocities are shown in Fig. 5. One can see that a certain amount of tracer mass may be retained near the symmetry axis (x-axis) and around the well when the regional groundwater velocity is relatively low, such as v_d=1×10^{-6} m/s and 1.5×10^{-6} m/s, as shown in Figs.5a-5b, resulting in relatively high concentrations in the wellbore at early stage. On the contrary, a larger regional groundwater velocity leads to a faster tracer transport process, causing the tracer mass drifting away from the well, as shown in Figs.5c-5d. Besides, one can also see that a larger regional groundwater velocity leads to a smaller distance from Sp to well, resulting in a smaller portion of tracer mass that can be extracted during the pumping phase. The opposite is true for the case of a smaller regional groundwater velocity. For instance, as for the tracer mass on the left side of the dividing streamline, they can be extracted by smaller velocities such as v_d=5×10^{-7} m/s and 1×10^{-6} m/s, as shown in Figs.5a-5b, but very limited tracer can be captured with larger velocities like v_d=3×10^{-6} m/s. And this further confirms the reasonability of the BTC types in Fig. 3. In addition, the effects of the duration of the rest phase, porosity and dispersivity on BTCs have been analyzed in a supplementary material as references.

~~4.2 The effects of t_{res} on BTCs in the SWPP test~~

Fig. 6 shows BTCs for the pumping phase with different t_{res}, like 6, 12, 24, and 36 hr. Besides, α_L=0.1 m, v_d=3×10^{-6}m/s, Q_{inj}=30 m^3/d, Q_{pump}= 15 m^3/d and the other parameters are the same as those used in Table 1. It is found that the tracer concentration is smaller as t_{res} increases in Fig. 6. This is because a longer time of rest phase means a farther distance of tracer drifting, leading to a smaller portion of tracer mass that can be extracted during the pumping phase. In order to interpret this behavior explicitly, the concentration distributions in a 2D horizontal plane at t_{pump}=0 hr with different t_{res} are shown in Fig. 7. One can see that a longer t_{res} means that more tracer mass drifting over the location of Sp toward downstream, resulting in lower concentrations in the wellbore during the pumping phase in Fig. 7. According to the analysis above, there is a strong interaction between regional groundwater flow and well flow, thus proper choices of the duration of each phase, and the injection and pumping rates are vital for the success of a SWPP test. For instance, for the case of a relatively large regional groundwater velocity, one can decrease t_{res} or increase the magnitude of Q_{pump} to recollect the tracer as much as possible, thus avoiding the over- or under-estimation of hydraulic parameters from the SWPP test.

4.3. The effects of porosity on BTCs in the SWPP test

Fig. 8 shows the effects of porosity θ on BTCs during the pumping phase. The parameters are given as: θ= 0.1, 0.2, 0.3, 0.4 and 0.5 respectively, v_d=3×10^{-6}m/s, α_L=0.1m, Q_{inj}=30 m^3/d, and Q_{pump}= 30 m^3/d. It can be found that the concentration is smaller at early stage with a smaller porosity. It is also obvious that a smaller θ will result in a longer tailing at late stage. The explanation is similar to that for Fig. 3, i.e., a smaller θ means a faster pore velocity, resulting in faster solute transport according to Eq. (3).

~~**4.4. The effects of dispersivity on BTCs in the SWPP test**~~

~~Fig. 9 shows the effect of α_L on BTCs for the pumping phase. The values of α_L are set as: α_L =0.01 m, 0.05 m, 0.1 m, 0.5 m and the other parameters are given as: v_d=2×10^{-6} m/s, Q_{inj}=30 m^3/d, and Q_{pump}= -30 m^3/d. As shown in Fig. 9, one can see that α_L has a significant impact on BTCs. At early stage of pumping, the concentration shows a decreasing trend with increase of α_L , This is because a larger dispersivity means a faster tracer transport , given the same regional groundwater velocity, which causes much broader solute plume after the injection and rest phases. A smaller dispersivity means a narrower solute plume. Therefore, different dispersivities can change the characteristics of BTCs under the influence of regional groundwater velocity.~~

~~4.5.~~4.2. The effects of skin hydraulic conductivity on BTCs in the SWPP test

As mentioned above, the well skin includes two general types, i.e., a positive skin or a negative skin. Denoting the hydraulic conductivities of skin and aquifer (or aquifer formation zone) respectively as K_s and K, one can use a new parameter $\delta=K_s/K$ to reflect the skin impact, where δ is a parameter reflecting the type of the skin and called the "skin index" hereinafter. Specifically, δ<1 represents a positive skin, while δ >1 represents a negative skin. Note that the case of δ =1 represents the case without a skin. In this section, we will provide a detailed analysis on the impact of the skin hydraulic conductivity on SWPP test.

~~**4.5.1 Positive skin**~~

Fig. ~~10~~ 6 shows the effect of different skin indexes on BTCs ~~for a positive skin case~~ during the pumping phase. The parameters are given as: v_d=3×10^{-6} m/s, Q_{inj}=30 m^3/d, Q_{pump}=-30 m^3/d, α_L=0.1 m, r_s=0.~~6~~ 7 m, δ= ~~1, 0.5, 0.25 and 0.125~~0.25, 0.5, 1, 1.5 and 2,

respectively. The results indicate that the concentration gets higher at early stage of pumping when the skin index is lower, as shown in Fig. ~~10~~6. This may be explained as follows. A skin with a lower δ value (or a lower permeability value in respect to that of the formation) essentially serves as a somewhat "shield" around the test well that can make the spreading of the tracer mass out of the test well more difficult during the injection phase. Consequently, more tracer mass will be retained near the test well either in the skin or near the skin ~~in the formation zone~~. Therefore, during the pumping phase of the test, more tracer mass can be extracted during the early stage of the pumping phase, leading to higher concentration during that stage. The facts are just the opposite for a larger δ value, this is because a negative skin (δ >1) is somewhat like a "high conductance zone" rather than a "shield", and can facilitate the spreading of tracer mass away from the test well during the injection phase. Therefore, less tracer mass will be retained near the test well for a higher skin index, thus less concentration will be seen during the early stage of pumping in the wellbore.

To further explicitly interpret this behavior, the concentration distributions in a 2D horizontal plane at t_{pump}=0 hr with different δ values are shown in Fig. ~~11~~7. As can be seen in Fig.~~11~~7, a lower δ value (or a lower skin hydraulic conductivity) ~~a lower skin hydraulic conductivity~~ leads to more tracer accumulation in the skin zone after the ~~rest~~ drift phase. On the contrary, it is quite obvious to see that a larger δ value (or a larger skin hydraulic conductivity) leads to a less tracer concentration in the skin zone at the early stage of the pumping phase. For instance, we can see that tracer accumulation in the skin zone for the cases of δ=2 is clearly less than the cases of δ=0.5 and 0.25. ~~For instance, one can see that the~~

~~solute plumes with high concentrations are clearly visible in skin zones for the cases of δ=0.25 and 0.125.~~

Fig. 8 displays the curves of concentration versus distance at t_{pump}=0 hr with δ= 0.25, 0.5, 1, 1.5 and 2, respectively. We can see that the concentration gets higher in the skin zone when the skin index δ is lower, as shown in Fig. 8. The results indicate that a lower skin hydraulic conductivity leads to more tracer accumulation in the skin zone after the drift phase~~further~~. The opposite is true if the skin index δ is larger. In addition, we can see that the peak of solute transport shorter distances at corresponding times with a lower δ value, results in the concentration gets higher at early stage of pumping as shown in Fig. 6. Therefore, the presence of the skin zone will lead to the variations of the concentration curves versus distance in the aquifer system.

~~**4.5.2 Negative skin**~~

~~Fig. 12 shows the effect of different skin indexes on the BTCs for a negative skin case. The parameters are given as: v_d=3×10^{-6}m/s, Q_{inj}= 30 m^3/d, Q_{ext}= 30 m^3/d, α_L=0.1 m, r_s=0.6 m, and δ=1, 1.5, 2 and 3 . In contract to what has been observed in Fig. 10 for a positive skin, the results indicate that the concentration gets lower at early stage of pumping when the skin index (δ) increases. This is because a negative skin is somewhat like a "high conductance zone" rather than a "shield", and can facilitate the spreading of tracer mass away from the test well during the injection phase. Therefore, less tracer mass will be retained near the test well for a higher skin index, thus less concentration will be seen during the early stage of pumping in the wellbore. Similar to what has been done for a positive skin in Fig. 11, the concentration~~

~~distributions in a 2D horizontal plane at t_{pump}=0 hr with different skin indexes are shown in Fig. 13. It is quite obvious to see that a larger skin hydraulic conductivity leads to a less tracer concentration in the skin zone at the early stage of the pumping phase. For instance, one can see that tracer accumulation in the skin zone for the cases of δ=2 and 3 are clearly less than the cases of δ=1 and 1.5.~~

~~4.6.~~4.3. Effects of skin thickness on BTCs in the SWPP test

In this section, we will analyze the impacts of the skin thickness on BTCs.

~~**4.6.1 Positive skin**~~

~~Firstly, we will analyze the impacts of the skin thickness on BTCs for a positive skin case.~~ The parameters are given as: v_d=3×10^{-6} m/s, Q_{inj}= 30 m^3/d, Q_{ext}=-30 m^3/d, δ= 0.5 (positive skin), δ= 2 (negative skin), α_L=0.1 m, and r_s= 0, 0.~~2~~3, ~~0.4~~ and 0.~~6~~7 m, respectively. For the case of δ= 0.5 (positive skin), one can see that the concentration gets higher at early stage with the increase of r_s in Fig. 9. ~~Fig. 14 shows the effects of the skin thickness (positive skin) on BTCs during the pumping phase. One can see that the concentration gets higher at early stage with the increase of r_s.~~ The explanation is similar to that for Fig. ~~10~~6, as a thicker positive skin means a thicker "shield" surrounding the test well, preventing the injected tracer mass from spreading further away from the test well, thus leading to higher concentrations during the early stage of the extraction phase. While for the case of δ= 2 (negative skin), it can be found that the concentration shows a decreasing trend with the increase of r_s, as a thicker negative skin means a thicker high conductance zone surrounding the test well, which will facilitate the spreading of injected tracer mass further away from the test well.

To further explicitly interpret this behavior, the concentration distributions in a 2D horizontal plane at t_{pump}=0 hr with different positive (or negative) skin thickness are shown in Fig. 10. ~~The concentration distributions in a 2D horizontal plane at t_{pump}=0 hr with different positive skin thickness are shown in Fig. 15.~~ It is evident that a larger positive skin thickness leads to more tracer accumulation in the skin zone after the drift phase. While for the case of negative skin, one can see that a greater portion of tracer mass migrates away from the test well after the cease of injection with a greater r_s in Fig. 10. For instance, one can see that tracer accumulation in the skin zone for the cases of r_s=0.7 and δ=2 is clearly less than the case of r_s=0.7 and δ=0.5.

~~the tracer mass still accumulates in the skin zone 24 hr after the cease of the injection phase (rest phase), and the concentration is higher in the skin zone than that in the formation zone (see the case of r_s=0.6 m). Besides, more tracer can be found in the skin region with the increase of r_s, resulting in different shapes of BTCs in Fig.14.~~

~~**4.6.2 Negative skin**~~

~~Similarly, we have also analyzed the impacts of the skin thickness on BTCs for a negative skin case. The parameters are given as: v_2=3×10^{-6} m/s, Q_{inj}= 30 m^3/d, Q_{ext}= 30 m^3/d, δ= 2 (negative skin), α_L=0.1 m, r_s=0, 0.2, 0.4 and 0.6m. Fig. 16 shows the effect of the skin thickness (negative skin) on BTCs during the pumping phase. At early stage, it can be found that the concentration shows a decreasing trend with the increase of r_s, and the peak values of BTCs also decrease with the increase of r_s. The explanation is similar to that for Fig. 12 as a thicker negative skin means a thicker high conductance zone surrounding the test well, which will facilitate the spreading of injected tracer mass further away from the test~

~~well. This is further supported by the concentration distributions in a 2D horizontal plane 24 hr after the cease of injection (rest phase) with different negative skin thickness, as shown in Fig.17. It is evident from Fig. 17 that a greater portion of tracer mass migrates away from the test well after the cease of injection with a greater r_s. For instance, at early stage of extraction, one can see that the BTC values in the case of r_s=0.6 m are lower than those in the case of r_s=0.2 m in Fig.16, and the tracer is transported further away from the test well in the case of r_s=0.6 m than that in the case of r_s=0.2 m in Fig.17.~~ Fig. 11 displays the curves of concentration versus distance at t_{pump}=0 hr with δ= 0.5 (positive skin), δ= 2 (negative skin), r_s= 0, 0.3, and 0.7 m, respectively. For the case of δ= 0.5 (positive skin), one can see that the concentration gets higher in the skin zone when ~~the~~ r_s is larger, as shown in Fig. 11. The results indicate that a thicker skin leads to more tracer accumulation in the skin zone after the drift phase ~~further~~ for a lower skin hydraulic conductivity. The facts are just the opposite for the case of negative skin. In addition, one can see that the peak of solute for a positive skin transport shorter distances at corresponding times with a thicker skin, results in the concentration gets higher at early stage of pumping as shown in Fig. 9. While for the case of a negative skin, the peak of solute transport ~~faster~~longer distances with a thicker skin. Therefore, different skin properties (skin type and thickness) will result in different shapes of BTCs in Fig.9.

4.4 Recovered tracer mass estimations

To allow for a more quantitative comparison between simulations, we have computed the ~~relative~~ratio of tracer mass recovered ~~by~~at the end of each SWPP test for different skin

properties (skin type and thickness). Such a ratio ~~Relative tracer mass recovered~~ can be can be written as:

$$\mu = \frac{m_{pump}}{m_{inj}} = \frac{\int_0^{t_{pump}} Q_{pump} \overline{C}_{pump} dt}{Q_{inj} t_{inj} C_0} \quad (26)$$

where, m_{inj} is the tracer mass injected during the injecting phase [M]; m_{pump} is the tracer mass recovered during the pumping phase [M]; μ is the percentage of recovered tracer mass in the injecting tracer mass [dimensionless].

According to ~~the~~ Fig. 9, the value the tracer concentration recovered was integrated from t_{pump} =0 to 48 hr, then we can obtain the tracer mass recovered for different skin properties, e.g. δ= 0.5 (positive skin), δ= 2 (negative skin), and r_s= 0, 0.2, and 0.6 m, respectively. Table 2 shows the percentage of recovered tracer mass in the injecting tracer mass for different skin properties. The results indicate that a lower δ value (or a lower permeability value in respect to that of the aquifer formation) leads to a larger ratio of tracer mass recovery ~~recovered, while the facts are just the opposite for a lower δ value~~. In addition, for the case of a positive skin, a larger r_s leads to larger ratio of tracer mass recovery ~~recovered~~, while the opposite is true for the case of a negative skin. In short, the skin properties (skin type and thickness) can result in different tracer mass recovery ratios~~ed~~.

4.5. Parameter estimations

As discussed in the above sections, the difference between the BTCs of the SWPP test under a skin and a non-skin is obvious. From a practical standpoint, hydrogeologists are interested in the accuracy of parameter estimation based on SWPP models, however, the phenomenon of skin effect is ~~unavoidable~~inevitable. Therefore, in the following, we will analyze ~~that~~ how the skin effect affects the estimation of aquifer properties such as

域代码已更改
域代码已更改
域代码已更改
域代码已更改

dispersivity, porosity and regional groundwater flow velocity, and the SWPP model with skin effect is chosen as the reference.

Now an interesting question is: what is the consequence if one adopts the non-skin SWPP model to interpret BTCs obtained from the model with skin? In another word, how different ~~is~~are the estimated parameters (e.g. dispersivity, porosity and regional groundwater velocity) ~~by~~ applying the non-skin SWPP model from their ‘‘actual” values based on the SWPP model with skin? If the differences between estimated and ‘‘actual” parameter values are not negligible, one can conclude that the skin effect should be taken into consideration when using the SWPP test model to estimate parameters. Fig. 12 shows BTCs at the well fitted by the non-skin model for different skin types (a positive skin or a negative skin). The “actual” parameters used in the SWPP model with skin are set as: v_d=3×10^{-6} m/s, Q_{inj}= 30 m^3/d, Q_{ext}=-30 m^3/d, δ= 0.5 (positive skin), δ= 2 (negative skin), α_L=0.1 m, θ =0.3 and r_s= 0.7 m, respectively. The circle lines are created by the numerical solution of the SWPP test with skin in three phases. The dashed lines are created by the non-skin SWPP test model. Using the trial-and-error method, we find that it is difficult to fit BTCs at the early stage of the SWPP test for a positive skin, but the fitness is good for a negative skin as shown in Fig. 12. Table 3 shows the parameter estimated by the non-skin model. One can see that ~~F~~for the case of a positive skin, both groundwater flow velocity and porosity estimated are smaller than their real values, and longitudinal dispersivity is larger than the real value based on the model with skin. In addition, for the case of a negative skin, groundwater flow velocity, porosity and longitudinal dispersivity estimated are larger than their real values based on the model with skin. In summary, the parameters estimated by the non-skin model are considerable different

from the real values, results in larger errors ~~under~~in parameter estimation if the non-skin model is mistakenly used when the skin presents~~ng parameters~~.

5. Conclusions

In this study, a numerical model for a SWPP test with the presence of a regional groundwater flow field, considering both the positive and negative skin effects was investigated. There is a strong interaction between regional groundwater flow and well flow, and various types of BTCs were analyzed for different regional groundwater velocity during pumping phase~~thus proper choices of the duration of each phase, and the injection and pumping rates should be done in advance before the SWPP test to recollect the tracer as much as possible~~. Besides, the numerical model of SWPP test can offer a way to estimate ~~be used to obtain~~ unknown parameters: i.e., regional groundwater velocity, effective porosity, and dispersivity~~, and biogeochemical reaction rates,~~ by fitting to the observed BTCs. The effects of both the hydraulic conductivities and thickness of the skin zone on BTCs had also been considered. The following conclusions can be drawn:

1. Regional groundwater velocity has a significant effect on the shape of BTCs, a lower regional groundwater velocity means that more tracer can be accumulated near the symmetry plane around the well. The opposite is true for a case of a larger regional flow velocity, resulting in a longer tailing of BTCs obtained during the extraction phase. In addition, the pattern and location of the dividing streamline determine the quantity of tracer mass extracted during the pumping phase.

2. We have proposed a skin index which is essentially the skin/formation hydraulic conductivity ratio to quantify the skin impact. A lager skin index results in a lower concentration for BTCs at early stage of pumping. On the contrary, a smaller skin index means a higher concentration for BTCs at early stage of pumping. A lager thickness of thea positive skin leads to a larger concentration of tracer near the symmetry plane around the well, but the facts are justand the opposite is true for the case of a negative skin. In addition, a smaller skin index means that solute plume can accumulate more in the skin zone, otherwise, a larger skin index results in a solute plume drifting further away from the skin zone after the cease of the injection phase.

3. The impact of skin effect near a pumping well should not be neglected for SWPP test, particularly when the regional groundwater flow is presented. The positive (or negative) skin results in a faster (or lower) tracer transport process. A lager thickness of the positive skin leads to a larger concentration of tracer near the symmetry plane around the well, but the opposite is true for the case with a negative skin. 3. The non-skin SWPP test model is used to interpret BTCs obtained from the model with skin, and the estimated parameters are very different from the ‘‘actual” values, results in larger errors in parameter estimation if the non-skin model is mistakenly used when the skin presents under estimating parameters. Therefore, the impact of skin effect near a pumping well should not be neglected for SWPP tests.

Acknowledgements

This research was partially supported by the National Natural Science Foundation of China (Grant Numbers: 41772259, 41372253, 41521001), the Natural Science Foundation of

Hubei Province, China (2018CFA085，2018CFA028), the Fundamental Research Funds for the Central Universities, China University of Geosciences (Wuhan). We appreciate the comments raised by ~~the~~ three anonymous reviewers and the Editor, which help us improve the quality of the paper substantially.

References

Benson, D. A., Tadjeran, C., Meerschaert, M. M., Farnham, I., and Pohll, G.: Radial fractional-order dispersion through fractured rock, Water Resour. Res., 40(12), 87-87, 2004.

Butler, A.P., Mathias, S.A., Gallagher, A.J., Peach, D.W., and Williams, A.T.: Analysis of flow processes in fractured chalk under pumped and ambient conditions (UK), Hydrogeol J., 17(8), 1849-1858, 2009.

Chen, C. S., and Chang, C. C.: Use of cumulative volume of constant-head injection test to estimate aquifer parameters with skin effects: Field experiment and data analysis, Water Resour. Res., 38(5), 189-195, 2002.

Chen, J. S., Chen, C. S., Gau, H. S., and Liu, C. W.: A two-well method to evaluate transverse dispersivity for tracer tests in a radially convergent flow field, J. Hydrol., 223(3-4), 175-197, 1999.

Chen, K.W., Zhan, H.B., and Yang, Q: Fractional models simulating non-fickian behavior in four-stage single-well push-pull tests, Water Resour. Res., 53(11), 9528-9545, 2017.

Drost, W., Klotz, D., Koch, A., Moser, H., Neumaier, F., and Rauert, W: Point dilution methods of investigating ground water flow by means of radioisotopes, Water Resour. Res., 4(1), 125-146, 1968.

Field, J. A., Sawyer, T. E., Schroth, M. H., Humphrey, M. D., and Istok, J. D.: Effect of cation exchange on surfactant-enhanced solubilization of trichloroethene, J. Contam. Hydrol., 46(1-2), 131-149, 2000.

Gelhar, L. W., and Collins, M. A.: General analysis of longitudinal dispersion in nonuniform flow. Water Resour. Res., 7(6), 1511-1521, 1971.

Guvanasen V., and Guvanasen V M.: An approximate semianalytical solution for tracer injection tests in a confined aquifer with a radially converging flow field and finite volume of tracer and chase fluid, Water Resour. Res., 23(8), 1607-1619, 1987.

Haggerty, R., Fleming, S. W., Meigs, L. C., and McKenna, S.A.: Tracer tests in a fractured dolomite: 2. Analysis of mass transfer in single-well injection-withdrawal tests, Water Resour. Res., 37(5), 1129-1142, 2001.

Hall, S.H., Luttrell, S.P., and Cronin, W.E.: A method for estimating effective porosity and ground-water velocity, Ground Water., 29(2), 171-174, 1991.

Hansen, S. K., Berkowitz, B., Vesselinov, V. V., O'Malley, D., and Karra, S. Push-pull tracer tests: their information content and use for characterizing non-fickian, mobile-immobile behavior, Water Resour. Res., 52(12), 9565-9585, 2016.

Hebig-Schubert, K.: Deep groundwater flow systems and their characterization in single-well settings by "push-pull" tracer tests, Int. J. Fatigue., 15(5), 441, 2014.

Huang, J. Q., Christ, J. A., and Goltz, M. N.: Analytical solutions for efficient interpretation of single-well push-pull tracer tests, Water Resour. Res., 46(8), 863-863, 2010.

Hurst, W., Clark, J. D., and Brauer, E. B.: Skin effect in producing wells, J. Petrol. Technol., 21(11), 1483-1489, 1969.

~~Istok, J. D., Humphrey, M. D., Schroth, M. H., Hyman, M. R., and O'Reilly, K. T.: Single-well "push-pull" test for in situ determination of microbial activities, Ground Water., 35(4), 619-631, 1997.~~

672 Kleikemper, J., Pelz, O., Schroth, M. H., and Zeyer, J.: Sulfate-reducing bacterial community
673 response to carbon source amendments in contaminated aquifer microcosms, Fems
674 Microbiol Ecol., 42(1), 109-118, 2002.
675 Johnsen, S. G., Whitson, C. H.: Analytical treatment of a push-pull "echo" test. Transp.
676 Porous Media, 77(3), 399. 2009.
677 Leap, D. I., Kaplan, P. G.: A single-well tracing method for estimating regional advective
678 velocity in a confined aquifer: Theory and preliminary laboratory verification. Water
679 Resour. Res., 24(7), 993-998, 1988.
680 Le Borgne, T., and Gouze, P.: Non-Fickian dispersion in porous media: 2. Model validation
681 from measurements at different scales, Water Resour. Res., 44(6), 2389-2393, 2008.
682 Michie, U.: The geological framework of the sellafield area and its relationship to
683 hydrogeology, Q. J. Eng. Geol., Hydroge. 29(Supplement_1), S13-S27, 1996.
684 Novakowski, K. S.: A composite analytical model for analysis of pumping tests affected by
685 well bore storage and finite thickness skin, Water Resour. Res., 25(9), 1937-1946, 1989.
686 Park, E. and Zhan, H. B.: Hydraulics of a finite-diameter horizontal well with wellbore
687 storage and skin effect, Adv. Water Resour., 25(4), 389-400, 2002.
688 Pickens, J. F., Jackson, R. E., Inch, K. J., and Merritt, W. F.:: Measurement of distribution
689 coefficients using a radial injection dual-tracer test, Water Resour. Res., 17(3), 529-544,
690 1981.
691 Paradis, C. J., Mckay, L. D., Perfect, E., Istok, J. D., and Hazen, T. C.: Push-pull tests for
692 estimating effective porosity: expanded analytical solution and in situ application.
693 Hydrogeol J 26(3), 1-13, 2018.

694 Schroth, M. H., Istok, J. D., and Haggerty, R.: In situ evaluation of solute retardation using
695 ingle-well push-pull tests, Adv. Water Resour., 24(1), 105-117, 2000.
696 Schroth, M. H. and Istok, J. D.: Models to determine first-order rate coefficients from single-
697 well push-pull tests, Ground Water., 44(2), 275-283, 2006.
698 Schroth, M. H., and Istok, J. D.: Approximate solution for solute transport during spherical-
699 flow push-pull tests, Ground Water., 43(2), 280-284, 2005.
700 Schubert, M., Brueggemann, L., Knoeller, K., and Schirmer, M.: Using radon as an
701 environmental tracer for estimating groundwater flow velocities in single-well tests,
702 Water Resour. Res., 47(3), 944-956, 2011.
703 Tong, M., Yuan, S., Ma, S., Jin, M., Liu, D., Cheng, D., and Wang, Y.: Production of
704 abundant hydroxyl radicals from oxygenation of subsurface sediments, Environ. Sci.
705 Technol., 50(1), 214-221, 2016.
706 Trudell, M. R., Gillham, R. W., and Cherry, J. A.: An in-situ study of the occurrence and rate
707 of denitrification in a shallow unconfined sand aquifer, J. Hydrol., 83(3), 251-268, 1986.
708 Wang, C. T., Yeh, H. D., and Tsai, C. S.: Transient drawdown solution for a constant
709 pumping test in finite two-zone confined aquifers, Hydrol. Earth Syst. Sci. Discuss.,
710 16(2), 441-449, 2012.
711 Wang, Q., Zhan, H., and Wang, Y.: Single-well push-pull test in transient forchheimer flow
712 field, J. Hydrol., 549, 125-132, 2017.
713 Wen, Z., Zhan, H. B., Huang, G. H., and Jin, M. G.: Constant-head test in a leaky aquifer
714 with a finite-thickness skin, J. Hydrol., 399(3-4), 326-334, 2011.

715 Yeh, H. D., Yang, S. Y., and Peng, H. Y.: A new closed-form solution for a radial two-layer
716 drawdown equation for groundwater under constant-flux pumping in a finite-radius well,
717 Adv. Water Resour., 26(7), 747-757, 2003.
718 Zimmermann, G., and Huenges, E.: Rock permeability and fluid pressure at the KTB.
719 implications from laboratory-and drill hole-measurements, Oil. Gas. Sci. Technol.,
720 54(6), 689-694, 1999.

Figure Captions:

Fig.1 The schematic diagram of the flow system. s_1, s_2, s_3 and s_4 are the boundaries of the model, and s_1 and s_2 are constant-head boundaries; both s_3 and s_4 are no-flux boundaries;

Fig.2 Comparison between the numerical solutions of this study and the analytical solutions of Huang et al. (2010).

Fig.3 BTCs for different values of v_d at the well during the pumping phase.

Fig.4 The schematic diagram of the flow system nearby well for the pumping phase.

Fig.5 Concentration distributions in a 2D horizontal plane at t_{pump}=0 hr. a) $v_d = 1\times10^{-6}$ m/s, b) $v_d = 1.5\times10^{-6}$m/s; c) $v_d = 2\times10^{-6}$ m/s; d) $v_d = 3\times10^{-6}$ m/s.

~~Fig.6 BTCs for different values of t_{res} at the well during the pumping phase.~~

~~Fig.7 Concentration distributions in a 2D horizontal plane at t_{pump}=0 hr. a) t_{res} = 6 hr; b) t_{res} = 126 hr; c) t_{res} = 24 hr; d) t_{res} = 36 hr.~~

~~Fig.8 BTCs at the well during the pumping phase with θ=0.1, 0.2, 0.3, 0.4, 0.5.~~

~~Fig. 9 BTCs at the well during the pumping phase with α_L=0.01 m, 0.05 m, 0.1 m, 0.5 m.~~

Fig. ~~10~~ 6 BTCs for different skin hydraulic conductivities~~for the case of a positive skin~~ at the well during the pumping with r_s=0.~~6~~ 7 m, and δ= ~~1, 0.5, 0.25 and 0.125~~0.25, 0.5, 1, 1.5 and 2.

Fig.~~11~~ 7 2D horizontal plane distributions of concentration ~~for a positive skin~~ with r_s=0.~~6~~ 7 m at t_{pump}=0 hr. a) δ= ~~1~~0.25; b) δ= 0.5; c) δ= ~~0.25~~1; d) δ= ~~0.125~~1.5; e) δ= 2.

Fig.8 Curves of concentration versus distance at t_{pump}=0 hr with δ= 0.25, 0.5, 1, 1.5 and 2.

~~Fig. 12 BTCs for the case of a negative skin at the well during the pumping with r_s=0.6 m, and δ= 1, 1.5, 2 and 3.~~

~~Fig.13 2D horizontal plane distributions of concentration for a negative skin with r_s=0.8 m at t_{pump}=0 hr. a) δ= 1; b) δ= 1.5; c) δ= 2; d) δ= 3.~~

Fig. ~~14~~ 9 BTCs for different skin indexes δ ~~the case of a positive skin~~ at the well during the pumping phase with r_s=0 m, 0.~~2~~ 3 m, and ~~0.4 m,~~ 0.~~6~~ 7 m.

Fig.1~~5~~0~~–~~ 2D horizontal plane distributions of concentration for different skin indexes δ at t_{pump}=0 hr~~Concentration distributions for a positive skin at 2D horizontal plane after 24 hr of rest~~. a) r_s =0.7 m, δ=0.5~~r_s= 0 m~~; b) r_s =0.3 m, δ=0.5~~r_s= 0.2 m~~; c) r_s= ~~0.4~~0 m; d) r_s= ~~=~~0.3 m, δ=2~~0.6~~ m; e) r_s =0.7 m, δ=2.~~.~~

Fig.11 Curves of concentration versus distance for different skin indexes δ at t_{pump}=0 hr with r_s=0 m, 0.3 m, and 0.7 m.

Fig.12 BTCs at the well fitted by the non-skin model for different skin indexes δ with r_s =0.3 m, δ= 0.25 and 2,

755 Table 1. The parameter values used in this study

Parameter name	Symbols	Values
Aquifer thickness (m)	B	10
Radius of well screen (m)	r_w	0.1
Density of groundwater(kg/m^3)	ρ	1000
Effective porosity of aquifer	θ	0.3
Hydraulic conductivity of aquifer (m/d)	K	8
Constant heads of S_1(m)	H_1	15.22, 15.44, 15.69, 15.65, ,15.87, 16.08, 16.30
Constant head of S_2 (m)	H_2	15.0
Regional groundwater Darcy velocities (m/s)	v_d	~~,~~5×10^{-7}, 1×10^{-6}, 1.5×10^{-6}, 2×10^{-6}, 2.5×10^{-6}, 3×10^{-6}
Longitudinal dispersivities of aquifer (m)	α_L	~~0.01, 0.05,~~ 0.1~~, 0.5~~
Hydraulic conductivity of skin zone (m/d)	K_s	~~1,~~ 2, 4, 12, 16~~,~~ ~~24~~
Effective porosity of skin zone	θ_s	~~0.21~~,0.24,0.27,0.33,0.36~~,0.39~~
Skin radius (m)	r_s	0.3, 0.7
Injection or pumping rate (m^3/d)	Q	15, 30
Mass flux per unit area (kg/(m^2 • s))	N_0	0.02765, 0.5529

Injection time (hr)	t_{inj}	6
Rest time (hr)	t_{res}	24
Pumping time (hr)	t_{pump}	48

Table 2. The relative tracer mass recovered by the end of each SWPP test

types	positive skin δ=0.5, r_s=0.7	positive skin δ=0.5, r_s =0.3	non-skin	negative skin δ=2, r_s =0.3	negative skin δ=2, r_s =0.7
μ (%)	0.95	0.85	0.83	0.82	0.74

762 Table 3. Parameter estimated by SWPP test model without skin

	Real values used in the model with skin	Estimated by the model without skin	
		positive skin(δ=0.5)	negative skin(δ=2)
α_L (m)	α_L=0.1	14α_L	17α_L
θ(dimensionless)	θ=0.3	0.5θ	1.53θ
v_d (m/s)	v_d=3.0×10^{-6}	0.6v_d	1.47v_d

763

764

765

766

767

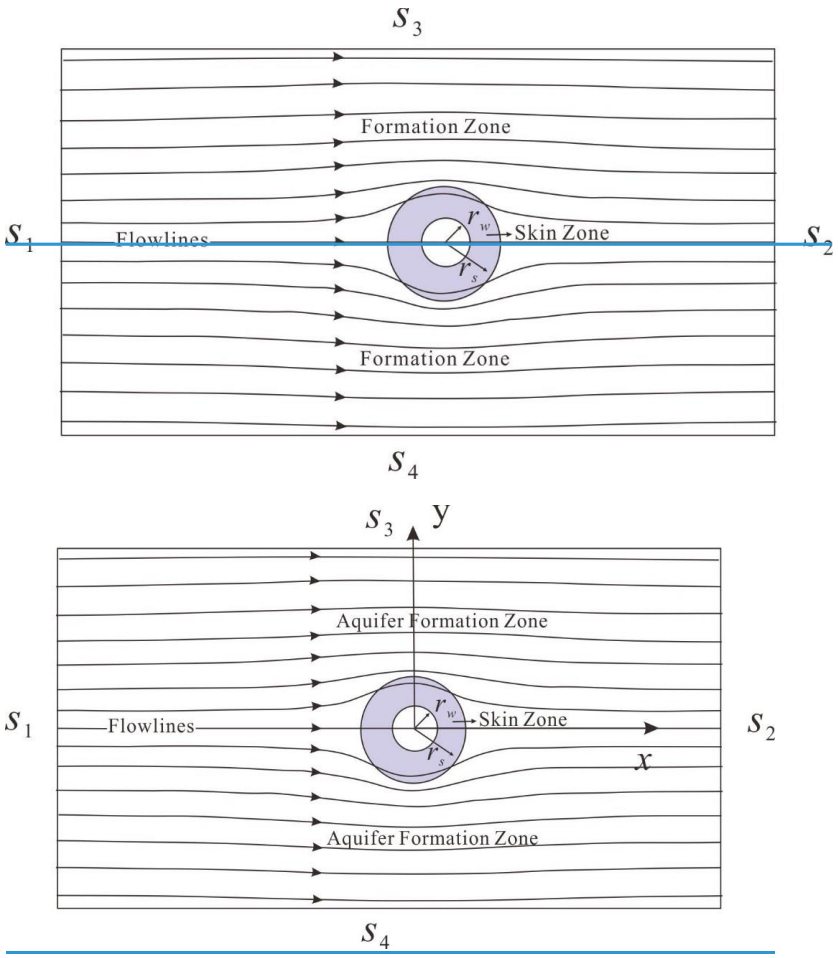

768

769

770

771

772

773 **Fig.1**

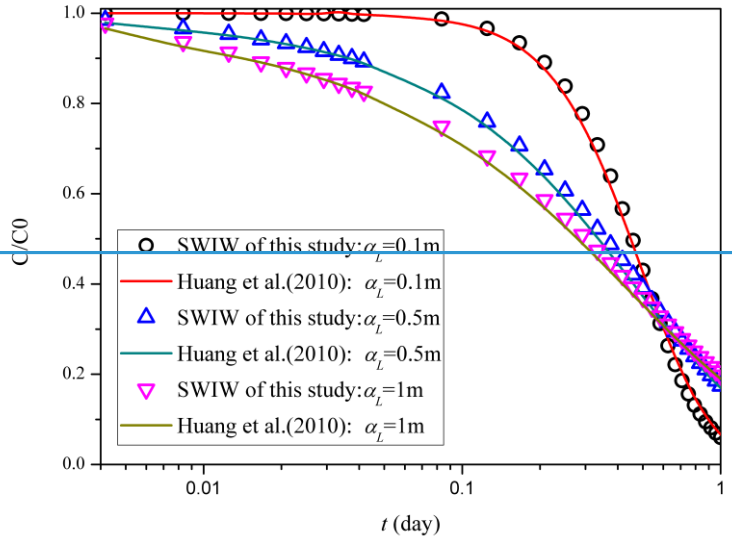
C/C0
t (day)
SWIW of this study:α_L=0.1m
Huang et al.(2010): α_L=0.1m
SWIW of this study:α_L=0.5m
Huang et al.(2010): α_L=0.5m
SWIW of this study:α_L=1m
Huang et al.(2010): α_L=1m

774

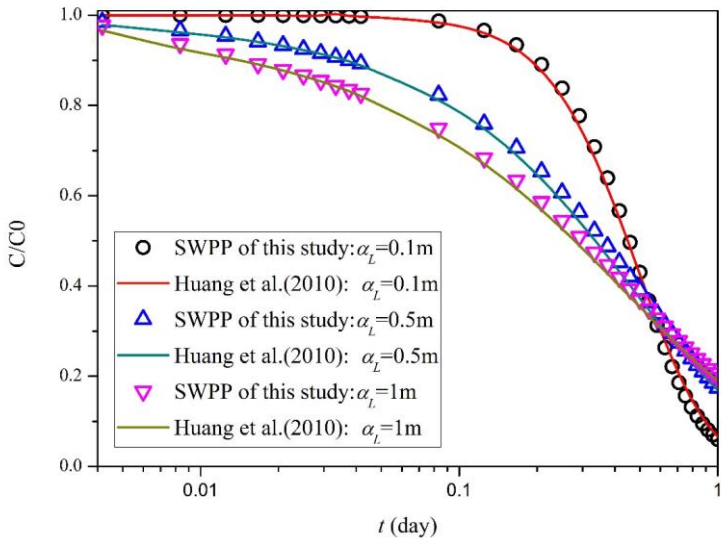
C/C0
t (day)
SWPP of this study:α_L=0.1m
Huang et al.(2010): α_L=0.1m
SWPP of this study:α_L=0.5m
Huang et al.(2010): α_L=0.5m
SWPP of this study:α_L=1m
Huang et al.(2010): α_L=1m

775

776

777

778

779

780 **Fig.2**

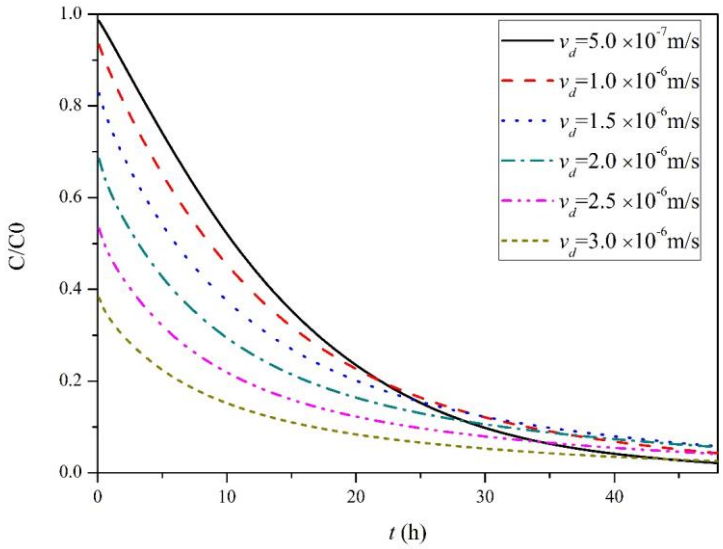

781

782

783

784

785 **Fig.3**

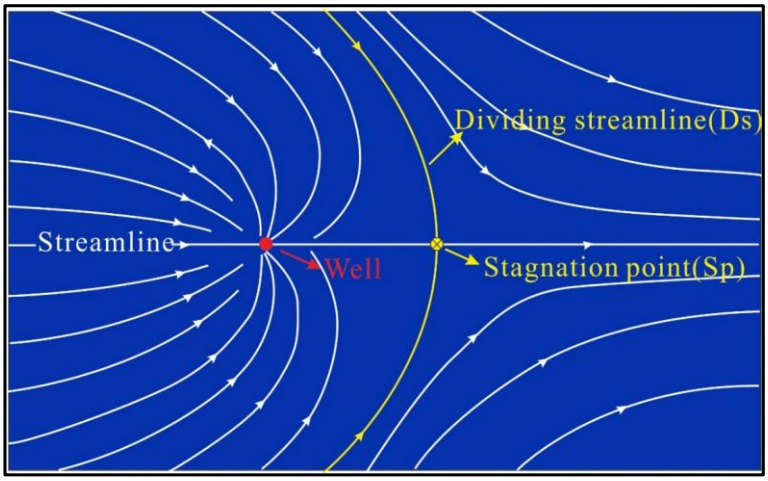

786

787

788

789

790

791

792 Fig.4

793

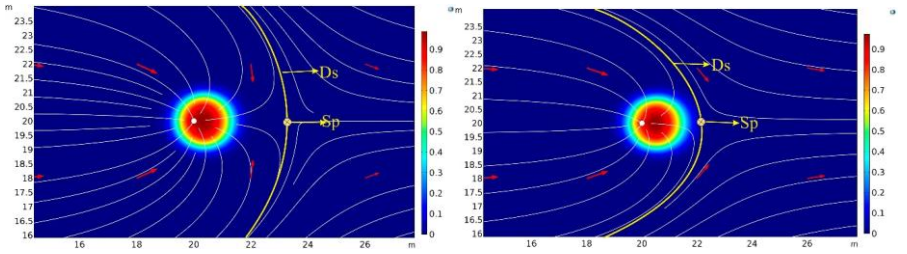

a. v_d=1e-6m/s b. v_d=1.5e-6m/s

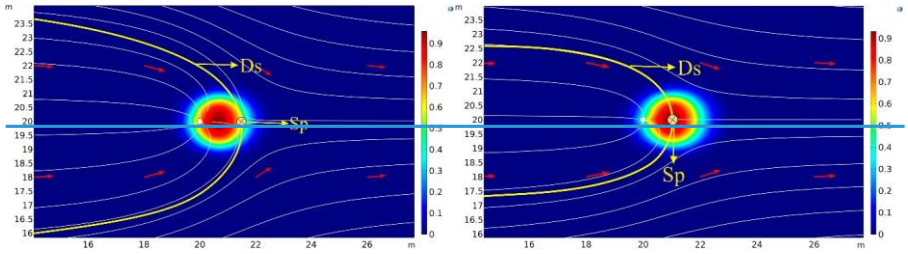

c. v_d=2e-6m/s d. v_d=3e-6m/s

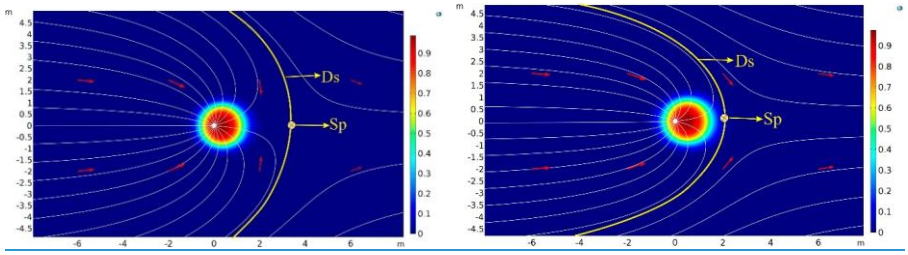

a. v_d=1e-6m/s b. v_d=1.5e-6m/s

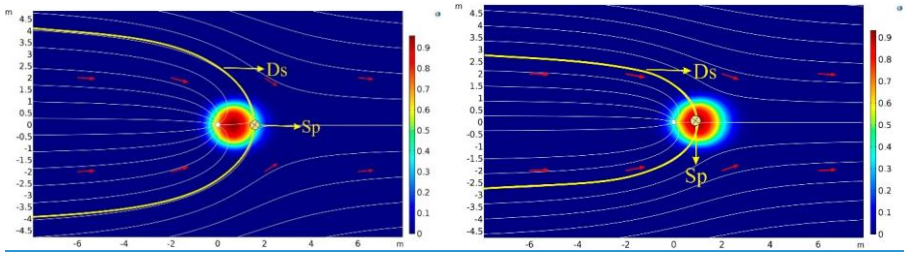

c. v_d=2e-6m/s d. v_d=3e-6m/s

Fig.5

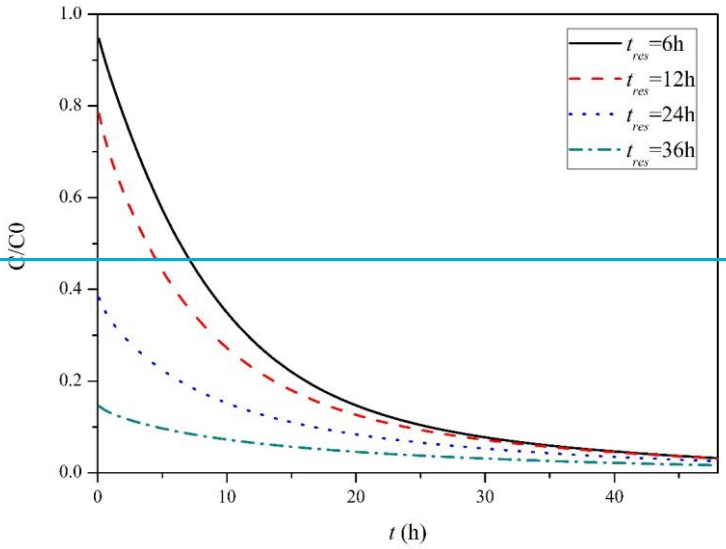

804

805

806

807 ~~Fig.6~~

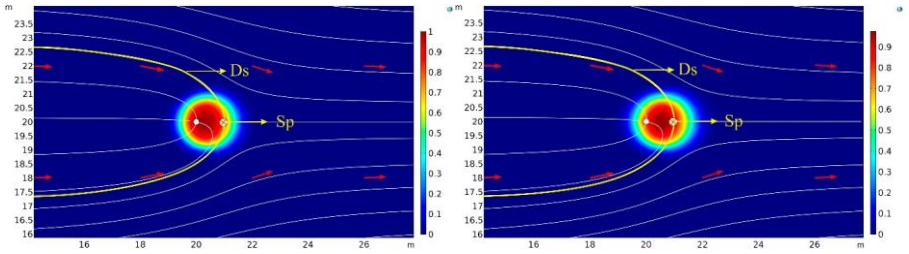

a. t_{res}= 6h b. t_{res}= 12h

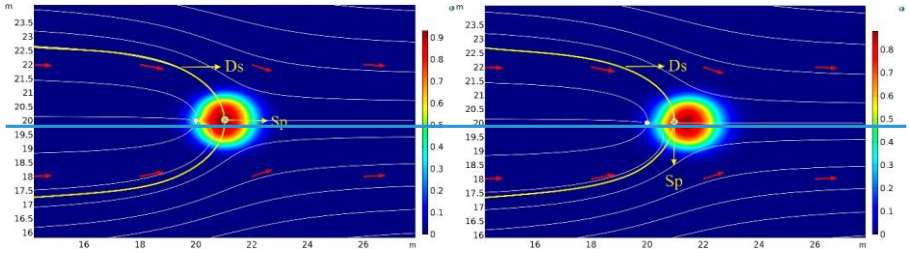

c. t_{res}= 24h d. t_{res}= 36h

Fig.7

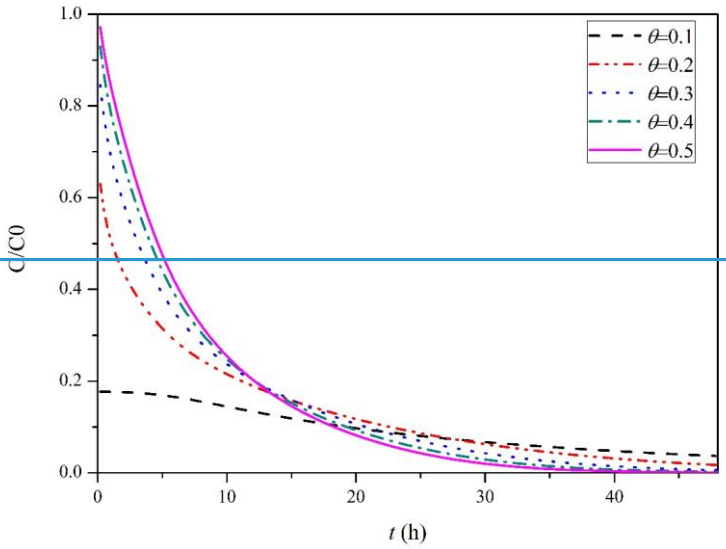

817

818

819

820 Fig.8

821

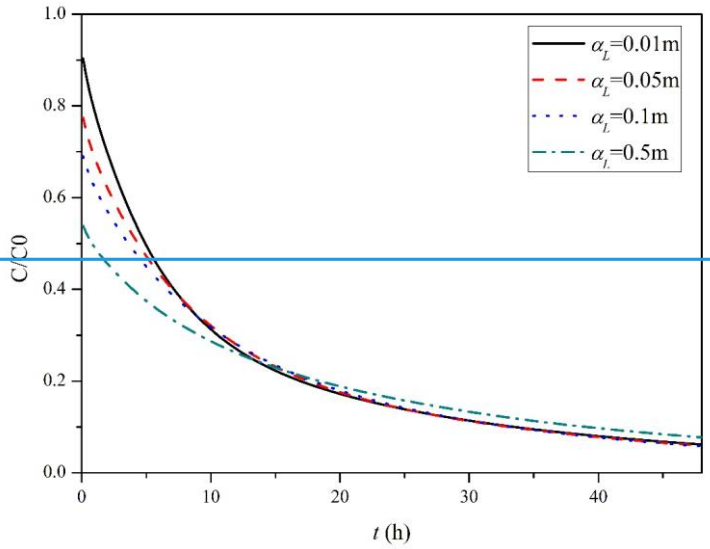

822

823

824

825 **Fig. 9**

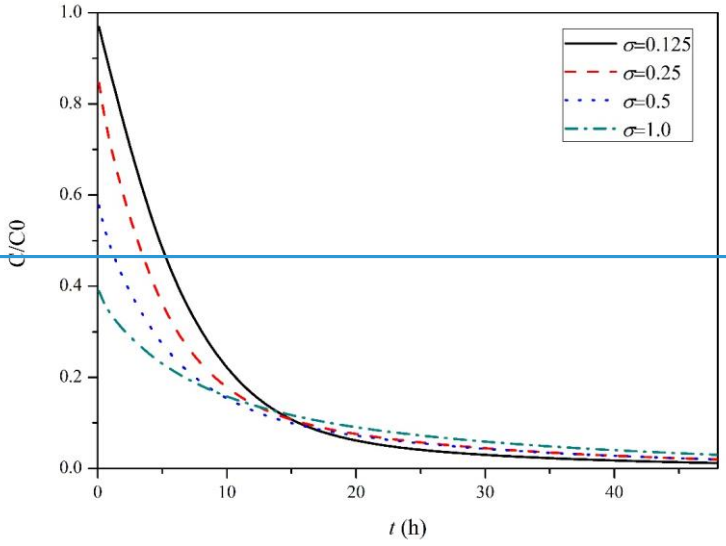

826

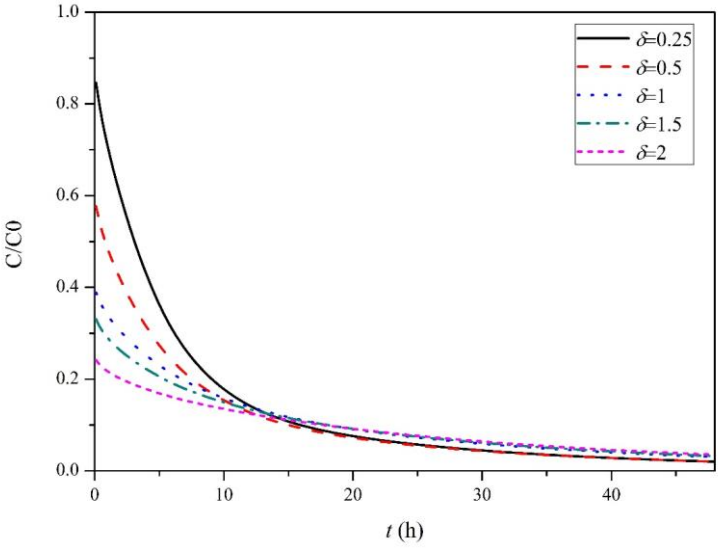

827

828

829

830

831 **Fig.~~10~~6**

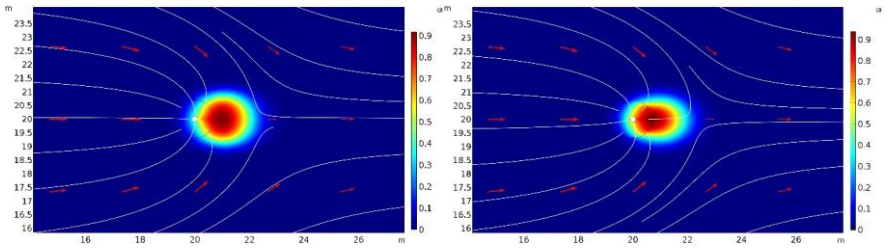

a. δ=1 b. δ=0.5

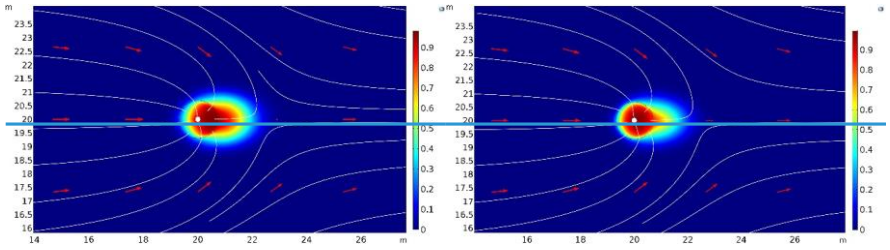

c. δ=0.25 d. δ=0.125

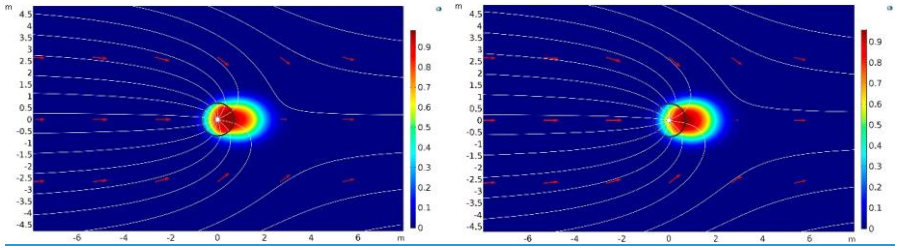

a. δ=0.25 b. δ=0.5

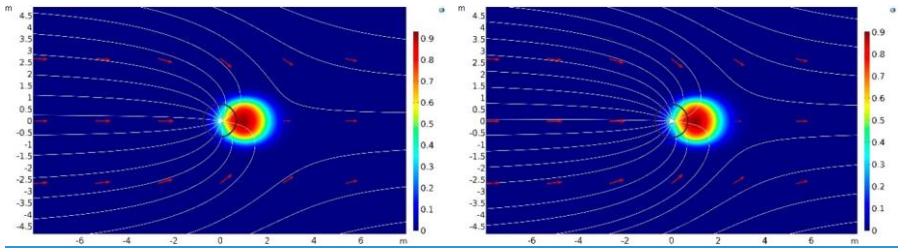

c. δ=1 d. δ=1.5

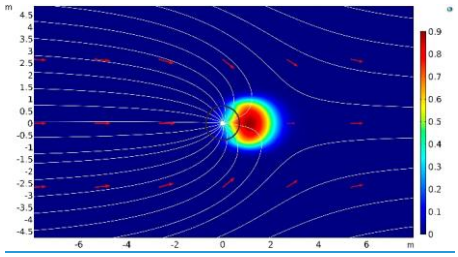

e. δ=2

Fig.~~11~~7

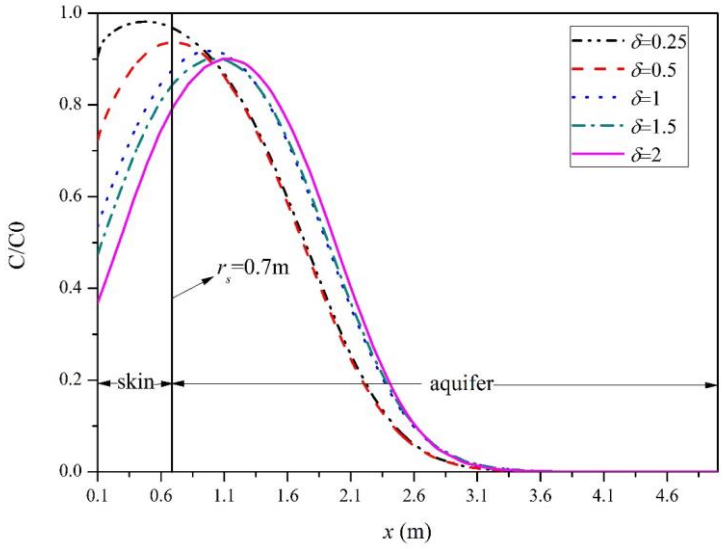
1.0
0.8
0.6
0.4
0.2
0.0
C/C0
0.1
0.6
1.1
1.6
2.1
2.6
3.1
3.6
4.1
4.6
x (m)
δ=0.25
δ=0.5
δ=1
δ=1.5
δ=2
r_s=0.7m
skin
aquifer

Fig.8

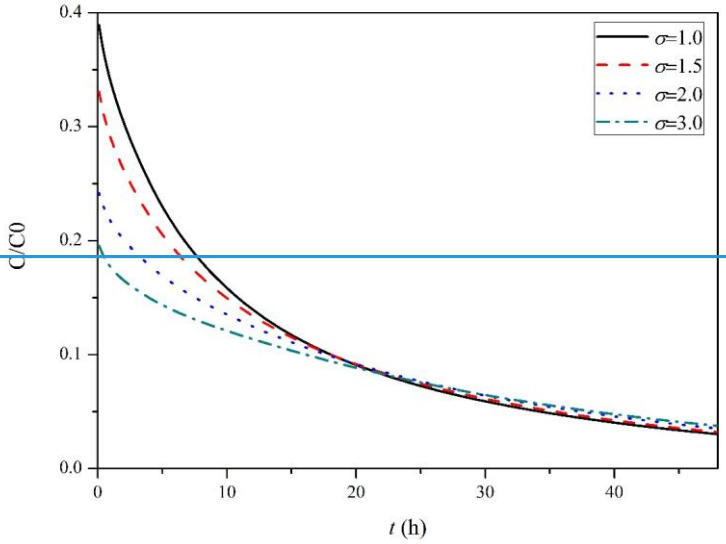

Fig.12

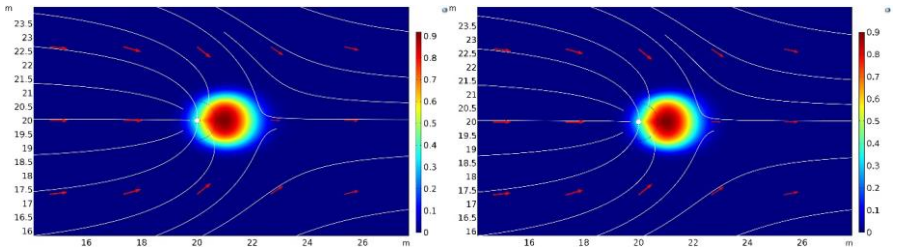

a. δ=1 b. δ=1.5

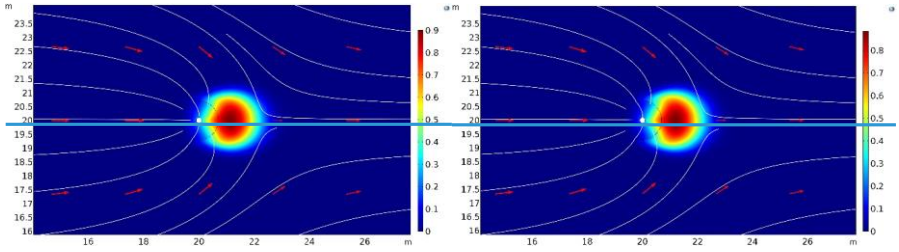

c. δ=2 d. δ=3

Fig.13

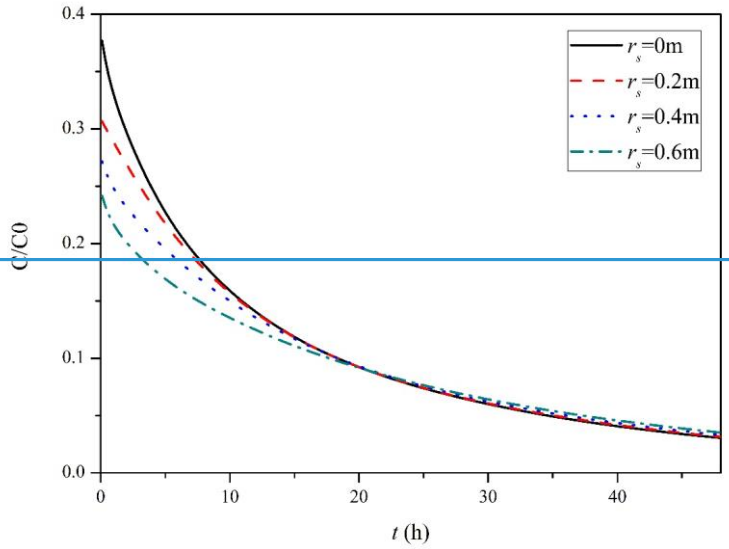
0.4
0.3
0.2
0.1
0.0
C/C0
0
10
20
30
40
t (h)
r_s=0m
r_s=0.2m
r_s=0.4m
r_s=0.6m

863

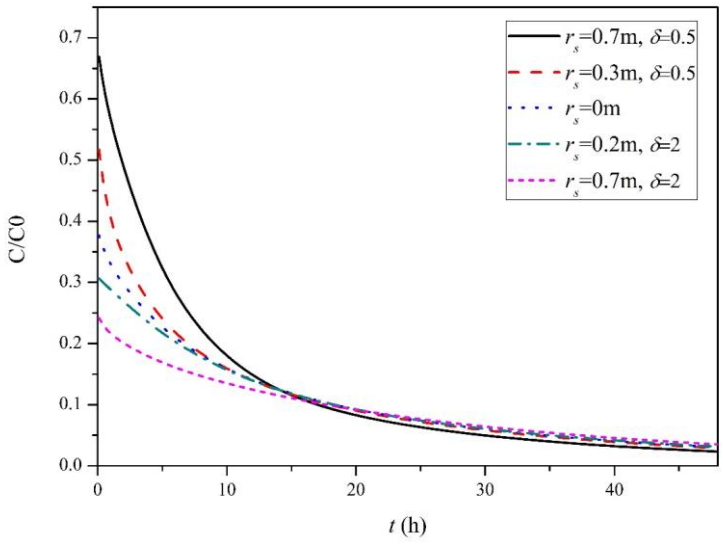
0.7
0.6
0.5
0.4
0.3
0.2
0.1
0.0
C/C0
0
10
20
30
40
t (h)
r_s=0.7m, δ=0.5
r_s=0.3m, δ=0.5
r_s=0m
r_s=0.2m, δ=2
r_s=0.7m, δ=2

864

865

866

867

868

869 **Fig.~~14~~9**

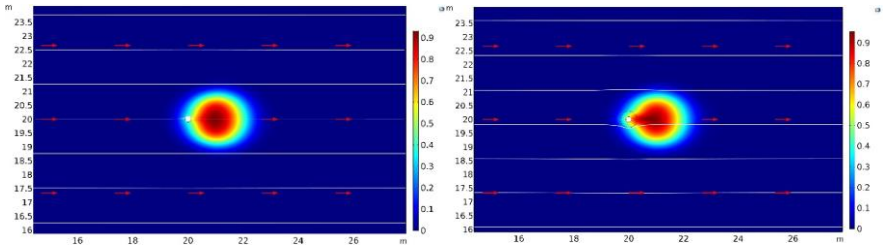

a. r_s =0 m b. r_s =0.2 m

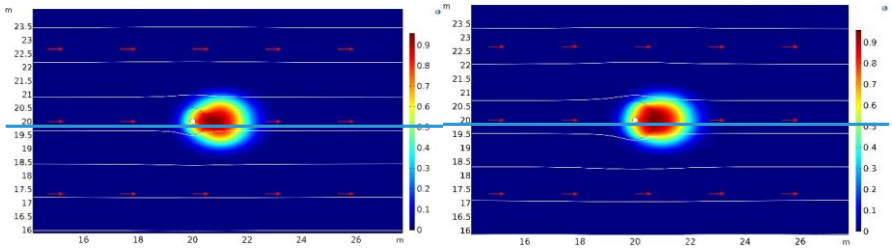

c. r_s =0.4 m d. r_s =0.6 m

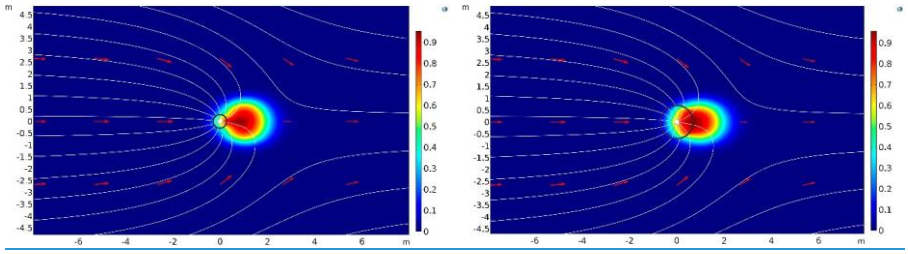

a. r_s =0.7 m, δ=0.5 b. r_s =0.3 m, δ=0.5

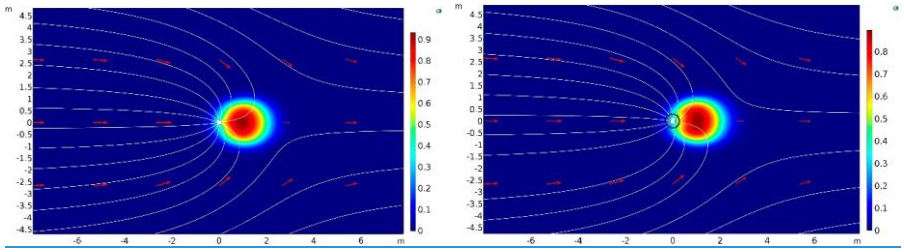

c. r_s =0 d. r_s =0.3 m, δ=2

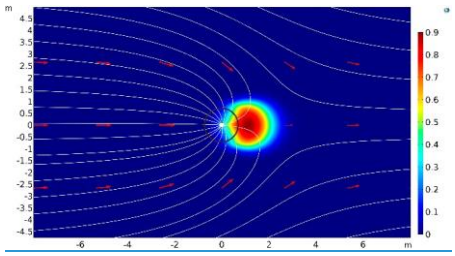

e. r_s =0.7 m, δ=2

Fig.10

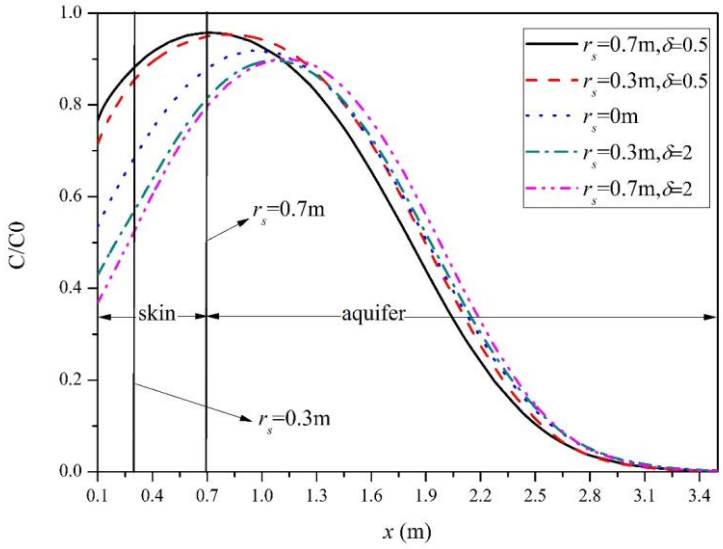
1.0
0.8
0.6
0.4
0.2
0.0
C/C0
0.1
0.4
0.7
1.0
1.3
1.6
1.9
2.2
2.5
2.8
3.1
3.4
x (m)
r_s=0.7m,δ=0.5
r_s=0.3m,δ=0.5
r_s=0m
r_s=0.3m,δ=2
r_s=0.7m,δ=2
r_s=0.7m
skin
aquifer
r_s=0.3m

Fig.11

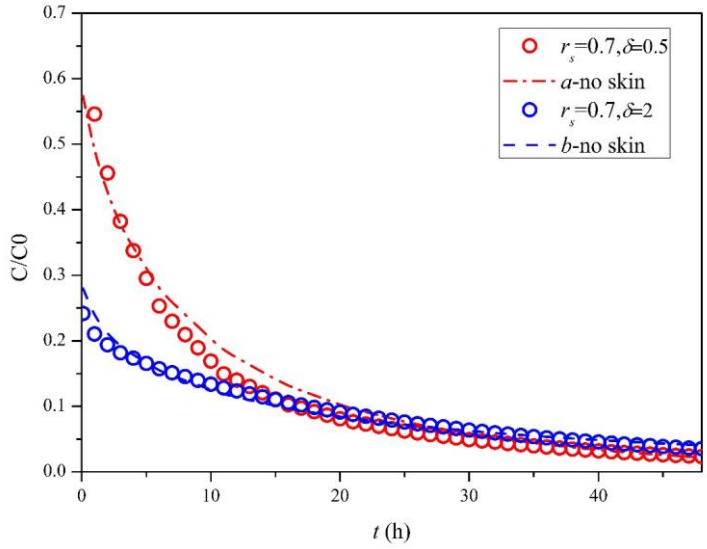

892

893

894

895

896 Fig.12

897

898

899

900

901

902

903

904

905 ~~Fig.15~~

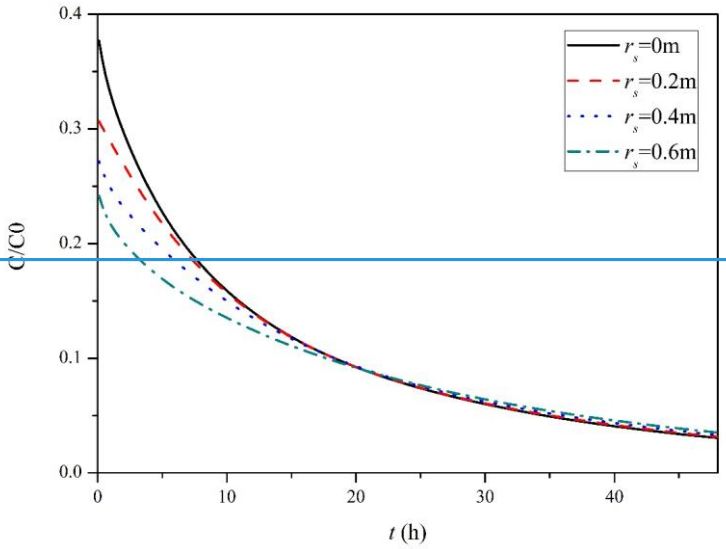

906

907

908

909

910 **Fig. 16**

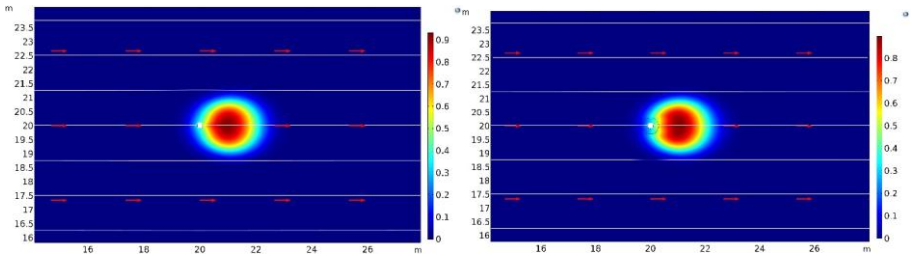

a. r_s =0 m b. r_s =0.2 m

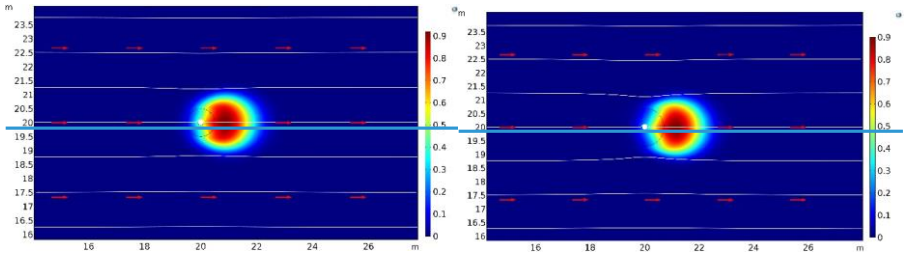

c. r_s =0.4 m d. r_s =0.6 m

Fig. 17